Research Article | Vol. 29, No. 19 / 13 Sep 2021 / Optics Express 30715
Optics EXPRESS

Amplification of stimulated light emission in arrays of nanoholes by plasmonic absorption-induced transparency

SERGIO G RODRIGO[1,2,*]

[1]Centro Universitario de la Defensa, Carretera Huesca s/n, 50090 Zaragoza, Spain
[2]Instituto de Nanociencia y Materiales de Aragón (INMA), CSIC-Universidad de Zaragoza, 50009 Zaragoza, Spain
[*]sergut@unizar.es

Abstract: Absorption induced transparency is an optical phenomenon that occurs in plasmonic nanostructures when materials featuring narrow lines in their absorption spectra are deposited on top of it. First reported in the visible range for metallic arrays of nanoholes, using dye lasers as covering, it has been described as transmission peaks unexpectedly close to the absorption energies of the dye. In this work, amplification of stimulated light emission is numerically demonstrated in the active regime of absorption induced transparency. Amplification can be achieved in the regime where the dye laser behaves as a gain material. Intense illumination can modify the dielectric constant of the gain material in a short span of time and thus the propagation properties of the plasmonic modes excited in the hole arrays, providing both less damping to light and further optical feedback that enhances the stimulated emission process.

1. Introduction

Lasers are ubiquitous devices in technology with strong presence in our everyday life [1]. The idea of down-scaling lasers to the nanoworld sparked the imagination of scientists since the beginning of lasers. Nanotechnology cleared the way to this goal, in part supported by a plenty of discoveries in the field of plasmonics. Plasmonics exploits a great variety of electromagnetic (EM) modes that are bound to the nanostructures in subwavelength volumes. In metals the strong confinement of light is due to Surface Plasmon Polaritons (SPP). The phenomena in which surface plasmons are involved are many and of a very diverse nature. For instance, in the quest of nanolasers metals and colloidal solutions of quantum dots have been combined to recently demonstrate plasmonic distributed-feedback lasers [2], and dye molecules, metals and silica-based photonic crystals have been used to create a 3D plasmonic laser [3].

Plasmonic lasers, that is *spasers*, require not just of a gain material to work but also of platforms that provide the necessary feedback to build the lasing action. Lattices of metallic nanoobjets (e.g. nanoparticles deposited on a substrate or holes drilled on metal films) are among the basic blocks for laser operation at the nanoscale. These are able to concentrate light in very hot spots distributed across the whole lattice size, forming regular patterns. Such systems have been reported to generate loss compensation, amplification and lasing of plasmons in metallic arrays of holes [4–9].

Regular arrangement on nanoobjects can give raise to emerging optical properties of the whole system that are not present in the constituent materials. These kind of structures are so-called metasurfaces and their optical response are described through effective theories, where the nanoobjects play the role of atoms. Metasurfaces are interesting for many applications in the extreme regime of light-matter interactions, where different forms of non-linear processes are present [10].

#436133 https://doi.org/10.1364/OE.436133
Journal © 2021 Received 7 Jul 2021; revised 23 Aug 2021; accepted 24 Aug 2021; published 8 Sep 2021

Optics EXPRESS

Here we investigate the gain response of a metasurface which collective behavior is due to the Absorption Induced Transparency (AIT) effect. AIT was discovered in arrays of nanoholes and was described as unexpected peaks in their transmission spectra, after the incorporation of a dye laser on the metal surface [11] . An opaque film (the metallic array of holes) becomes translucent after incorporation of the solution containing the dye laser. The physical mechanism was initially puzzle, as AIT occurred at frequencies of high absorption because the presence of the molecules.

Two physical mechanisms explain AIT. The first is due to strong modifications of the propagation constant of light inside the holes by the presence of the dye [12]. The second mechanism is related with the excitation of SPPs, ultra-confined at the layer where the molecules are located [13]. Both contribute to AIT and are related with other processes of light scattering by corrugated metal films, like Extraordinary Optical Transmission (EOT) [14].

The AIT phenomenon was observed in the visible range for the first time, although later on it was predicted to occur outside that frequency window [12]. The theoretical prediction was ultimately verified in the terahertz regime, where the role of the electronic transitions of the dye molecules in the visible was played by phonon resonances in LiF [15].

Apart from a few studies focused on fundamental aspects of light-matter interactions [16],the detection of gases in the THz regime [17] or for sensing applications at infrared via thermal effects [18], AIT has been elusive in many experiments. Let us say that only a few experiments focused in strong coupling found effects ascribed to AIT [19], while many others did not do in similar setup conditions [20,21].

In this work we theoretically demonstrate the amplification of stimulated light relying on active AIT. The rest of the work is organized as follows: the basic elements of the theoretical framework are discussed in Section 2, the main results devoted to AIT in the active regime are provided in Section 3 and, finally, we will end with the conclusions in Section 4.

2. Materials and methods

The dye laser IR-140, embedded in a host medium consisting in a polymer PMMA matrix with refractive index $n_h = 1.62$, has been chosen as the gain material to illustrate the principles of active AIT. This dye molecule has demonstrated to perform better than other dye lasers in terms of stability and photobleaching, which for IR-140 occurs at pumping energies as high as 0.8 mJ/cm^2, i.e., a few GW/cm^2 in the case of femtosecond lasers [7]. Our proposal is not constrained to the use of dye lasers, so different gain materials might be suitable, like quantum dot nanoplatelets that exhibit better lasing response that of dye lasers. [22]

The optical properties (including gain) of the IR-140 dye laser can be simulated using a four-level atomic model. Schematically shown in Fig. 1, IR-140 optical response is fully described by the following parameters (retrieved from Ref. [23]): absorption and emission wavelengths $\lambda_a = 805$ nm and $\lambda_e = 870$ nm; absorption and emission dipole strengths (coupling constants) $\sigma_a = 6.898 \times 10^{-8} C^2/kg$ and $\sigma_e = 5.152 \times 10^{-8} C^2/kg$; resonances half-width $\Gamma_a = 0.134$ fs^{-1} and $\Gamma_e = 0.075$ fs^{-1}. Finally, relaxation times are: $\tau_{32} = \tau_{10} = 100$ fs and $\tau_{21} = 240$ ps. The population of the ground state (density of the molecules) has been chosen so $N_0 = 0.6$ molecules/nm^3, which is similar to others reported in literature.

Our predictions are based on numerical calculations conducted with an own code of the Finite Difference Time Domain (FDTD) method, which provides a self-consistently approach for solving both Maxwell's and molecular-rate equations based on the Maxwell-Bloch formalism. A complete description of the Maxwell-Bloch formalism can be found in Ref. [24]. Details about our FDTD implementation can be found elsewhere [25]. The full temporal evolution of the population densities for a four-level system can be expressed as follows:

$$\frac{\partial N_3}{\partial t} = \frac{\vec{W}_a}{\hbar\omega_a}\vec{E}_{loc} - \frac{N_3}{\tau_{32}} \tag{1}$$

Optics EXPRESS

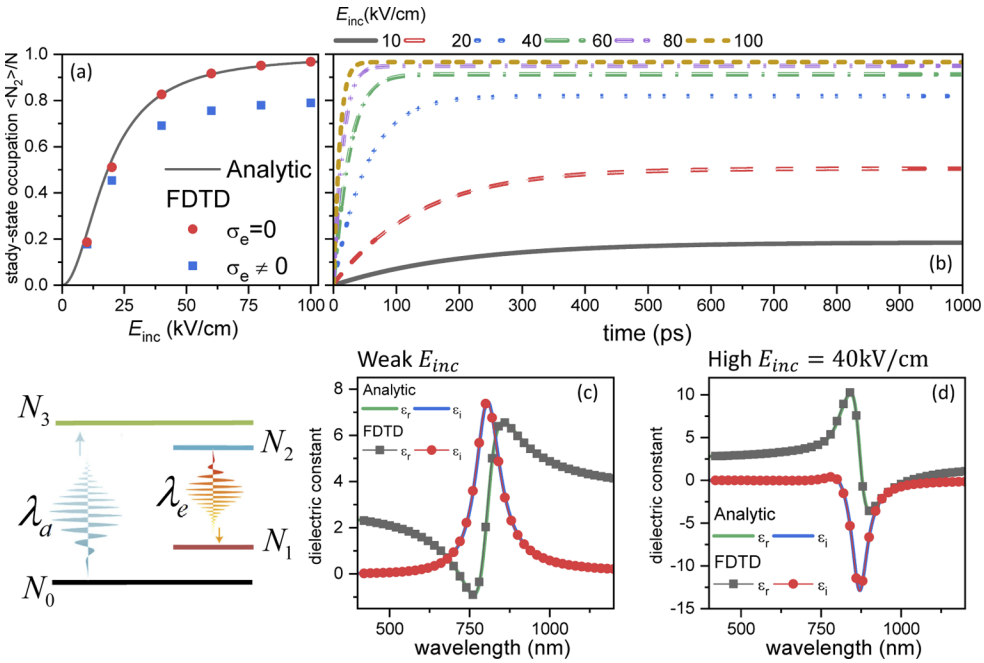

Fig. 1. The optical response of the infrared dye laser IR-140 used in this work as gain material can be approximated as a four-level atomic system, shown in the schematics (for further details, see main text). The simulated material consist of a polymeric matrix of PMMA where the IR-140 dye is introduced. The host medium has refractive index n_h =1.62. (a) Comparison between numerical simulations (symbols) and the analytic result (solid line) of the normalized steady-state occupation density of the upper emission state ($\langle N_2 \rangle / N$) in a 4 nm thin slab of gain material when continuously pumped by plane wave at λ_a = 805 nm, as a function of the electric field amplitude of the incident field. Square symbols are full calculations using Maxwell-Bloch equations, while circular symbols show and approximation where null overlap between emission and absorption bands is assumed. (b) For this approximation, time evolution of $\langle N_2 \rangle / N$ for different incident fields. (c)-(d) Steady-state dielectric constant ($\varepsilon_r + \imath\varepsilon_i$) inside the 4 nm thin slab of gain material for: (c) weak pumping and (d) intense illumination under an incident electric field of E_{inc} = 40 kV/cm, which produces a steady-state population of the emission state $\langle N_2 \rangle / N$ = 0.83, for σ_e = 0.

Optics EXPRESS

$$\frac{\partial N_2}{\partial t} = \frac{N_3}{\tau_{32}} + \frac{\vec{W}_e}{\hbar\omega_e}\vec{E}_{loc} - \frac{N_2}{\tau_{21}} \tag{2}$$

$$\frac{\partial N_1}{\partial t} = \frac{N_2}{\tau_{21}} - \frac{\vec{W}_e}{\hbar\omega_e}\vec{E}_{loc} - \frac{N_1}{\tau_{10}} \tag{3}$$

$$\frac{\partial N_0}{\partial t} = \frac{N_1}{\tau_{10}} - \frac{\vec{W}_a}{\hbar\omega_a}\vec{E}_{loc}, \tag{4}$$

where $N_i = N_i(\vec{r}, t)$ are the occupations of the different energy levels. The coupling factor, $\vec{W}_i = \frac{\partial \vec{P}_i}{\partial t} + \Gamma_i \vec{P}_i$, being $\vec{P}_i(\vec{r}, t)$ the polarization densities labeled as $i = a, e$ for absorption and emission respectively. The absorption and emission transitions are accessible to the local electric field, $\vec{E}_{loc} = [(2 + n_h^2)/3]\vec{E}$, in the Lorentz approximation through the polarizabilities:

$$\frac{\partial^2 \vec{P}_i}{\partial t^2} + 2\Gamma_i \frac{\partial \vec{P}_i}{\partial t} + \omega_i^2 \vec{P}_i = -\sigma_i \Delta N_i \vec{E}_{loc} \tag{5}$$

Here $\omega_i = \frac{2\pi c}{\lambda_i}$, $\Delta N_a = N_3(\vec{r}, t) - N_0(\vec{r}, t)$ and $\Delta N_e = N_2(\vec{r}, t) - N_1(\vec{r}, t)$.

The dielectric constant derived from the four-level atomic system is described by a sum of Lorentz terms, corresponding to absorption and emission electronic transitions, and it can be analytically expressed as follows:

$$\varepsilon(\omega) = \varepsilon_h + \frac{(2 + n_h^2)}{3}\frac{\Delta N_a}{\varepsilon_0}\frac{\sigma_a}{(\omega^2 - \Omega_a^2 + \imath 2\omega\Gamma_a)} + \frac{(2 + n_h^2)}{3}\frac{\Delta N_e}{\varepsilon_0}\frac{\sigma_e}{(\omega^2 - \Omega_e^2 + \imath 2\omega\Gamma_e)}. \tag{6}$$

This mathematical expression permits to obtain the local gain once the population levels are known by other means, for instance aid by the FDTD method.

Figure 1(a) shows the normalized steady-state occupation density of the upper emission state, $\langle N_2\rangle/N$, inside a 4 nm thin slab of gain material when continuously pumped by plane wave at $\lambda_a = 805$ nm, as a function of the electric field amplitude of the incident field. Square symbols are obtained with the full model given by Eq. (1)–(5). These equations can be approximated for a continuous wave illumination where the populations of interest are those of the steady-state. By doing so, the steady state occupation density of the upper emission state results in:

$$\langle N_2\rangle/N = \frac{1}{1 + 3\tau/\tau_{21} + |E_{sat}/E_{loc}|^2} \tag{7}$$

where $E_{sat}^2 = \frac{4\hbar\omega_a\Gamma_a}{\sigma_a\tau_{21}}$. This formula includes two additional approximations: the overlap of the emission band with the absorption spectrum is negligible ($\sigma_e = 0$) and $\tau = \tau_{32} = \tau_{10}$.

Applying Eq. (7) to the IR-140 dye results in the solid line of Fig. 1(a). To compare with the analytical results numerical simulations were conducted. In the same figure circles show $\langle N_2\rangle/N$ obtained with the Maxwell-Bloch equations, where null overlap between emission and absorption bands is imposed by setting $\sigma_e = 0$. In the case of IR-140 this approximation does not hold, its emission and absorption bands strongly overlap, as deduced by analyzing the steady-state values of the emission level for $\sigma_e \neq 0$, depicted with square symbols in Fig. 1(a). Interestingly, the steady-state values are reached at different moments for different incident intensities. Figure 1(b) shows the full time evolution of $\langle N_2\rangle/N$ for those values of the incident field analyzed in Fig. 1(a). As we can observe, the higher the intensity the faster the steady-state is reached. This information will be useful to determine the time delay between laser pulses in pump-probe numerical experiments, which will be presented later on.

Figure 1 also shows the dielectric constant calculated within the 4 nm thin slab of gain material (c) before and (d) after continuously pumping it with an intense laser beam ($E_{inc} = 40$ kV/cm) at

Optics EXPRESS

the absorption energy of the molecules. The analytical result given by Eq. (6) is represented with a solid line in each case. The steady-state population is $\langle N_2 \rangle / N = 0.83$ ($\sigma_e = 0$). Figure 1(c) shows the typical profile of a spectral absorption line: within the anomalous dispersion region, where phase velocity would exceed that of the speed of light, the material is forced to experience high absorption to do not break causality, which explain the peak in the imaginary part of the dielectric constant, ε_i. In contrast, anomalous dispersion disappears in Fig. 1(d) and ε_i<0, so optical gain through the suppression of losses is reached within the thin film.

The excellent agreement between numerical and analytical results highlights the validity of our numerical implementation. Equation (6) provides the dielectric response of the four-level system when the atomic populations are known. To obtain the results of Fig. 1(d) FDTD simulations were carried out. The numerical time-domain simulations conducted with the FDTD method highlight a crucial point. The steady-state occupation of the atomic levels is fundamental to grasp the details of the stimulated process that might eventually produce lasing. However, it is even more important to understand the dynamics of the atomic systems under investigation, specially when dealing with femtosecond pulses. One of the advantages of FDTD is that light pulses can be straightforwardly incorporated into the model because FDTD belongs to the class of time domain methods. In addition, the FDTD method is able to self-consistently treat gain materials in complex plasmonic heterostructures where the local EM field might abruptly change from point to point.

3. Results and discussion

We investigate the gain response of AIT metasurfaces with the numerical equivalent of a pump-probe spectroscopy experiment, as illustrated in the schematics shown in Fig. 2 and Fig. 3. The spectral position of the AIT peak, its intensity and spectral width are parameters mainly controlled by the propagation properties of light either inside the holes and on the surface (as propagating SPPs) [13]. We show that by acting on the characteristic wavevectors by means of a non-linear process active control of AIT is achieved.

Pump-probe numerical experiments have been conducted to show the effect of gain in AIT. The metasurface is first pumped with a 150 *fs* laser beam, central wavelength corresponding to the absorption energy of the IR-140 molecules. Finally, a second low power and spectrally broadband beam (the probe) is sent after Δt =800 *fs*. This time delay allows the probe hitting the system once the populations of IR-140 have reached the stationary state, considering the large relaxation time of the emission level (τ_{21} = 240 ps). The probe is weak enough so the atomic populations keep unaltered. Note that the scattering coefficients of Fig. 2 and Fig. 3 are that of the probe. The metallic substrate of the AIT metasurface is silver, its optical response taken from experimental tabulated values implemented in our FDTD code by means of a Drude-Lorentz model [26].

We will distinguish between localized and surface AIT. In localized AIT the molecules completely fill the holes (Section 3.1), whereas a 30 nm thin layer of them covers the metasurface in the case of surface AIT (Section 3.2).

3.1. Localized AIT

We start analyzing a bare structure (without the dye laser) designed for AIT, consisting on a metallic array of circular nanoholes (diameter, d = 180 nm; period, p = 250 nm; and metal thickness, h = 200 nm). Figure 2(a)-(b) shows the transmittance (T) and reflectance (R) obtained for such metasurface with black lines. The system behaves as a mirror. Once the dye fills the holes (there is no over layer) the metasurface begins featuring AIT, which is seen as a broadband spectral feature in the near infrared (red lines) of both transmission and reflection. The last results correspond to the probe scattering without pumping. As the intensity of the pump beam increases the population of the upper levels of the molecules increases too, changing the dielectric constant

Optics EXPRESS

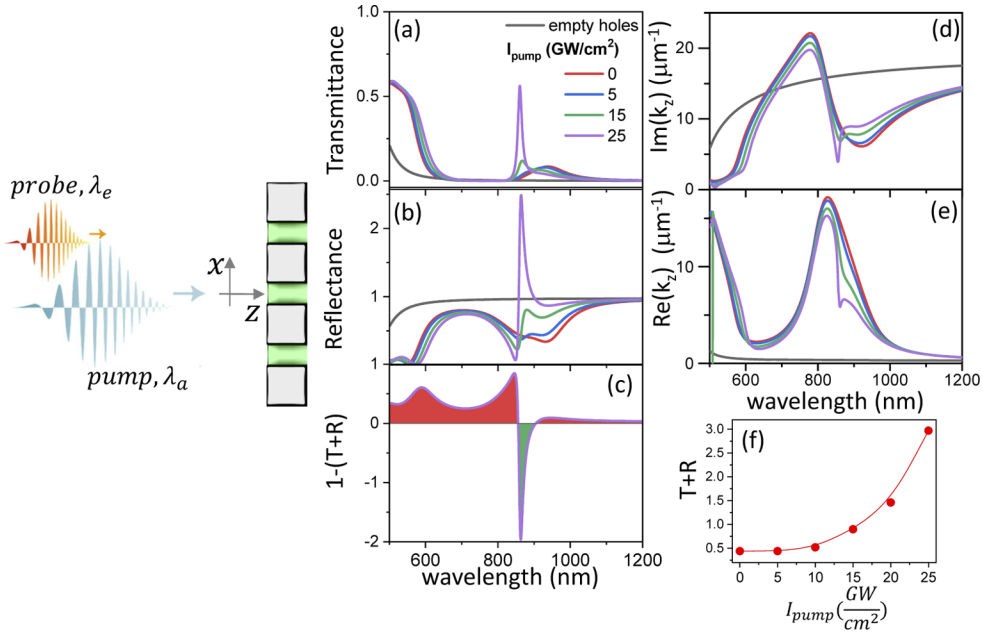

Fig. 2. Localized AIT: (a) Probe transmittance (T) and (b) reflectance (R) as a function of the pump intensity, for an AIT metasurface of circular holes (diameter, d = 180 nm) periodically arranged (period, p = 250 nm), on a silver film (thickness, h = 200 nm). The passive case (no IR-140 dye inside the holes) is shown with a solid black line.(c) Light absorbed/emitted by the AIT metasurface calculated as $1-(T+R)$, for the highest pump intensity. (d)-(e) The corresponding real and imaginary parts of the propagation constant of light inside the holes, k_z. (f) T+R calculated at λ = 864 nm (maximum of stimulated emission) as a function of the pump intensity.

of the dye laser as expected from Eq. (6). For that situation, the AIT peak evolves towards a narrow emission line centered at λ = 864 nm, near the emission energy of the dye laser. Spectral narrowing is one important condition that lasers must fulfill. Although we observe substantial spectral narrowing of the emitted light, further research is necessary to claim the existence of plasmonic lasing in these systems. Reflection is also affected by the optical gain and a peak shows up at the same energy. A nice figure of merit that measures the degree of gain deposited by the pump in the material is $1-(T+R)$, shown in Fig. 2(c). This quantity corresponds to absorption in the passive case, i.e., photons are lost from the incident field, so it is always a positive number. In the active situation energy in the matter states (the dye laser) can be released as photons that produces a negative absorption by means of stimulated light emission [27]. The red shaded regions are dominated by absorption. Into the green shaded region stimulated emission is taking place. This trend is markedly clearer at λ = 864 nm, energy at which photons at the light field substantially exceeds those delivered by the probe.

Enhanced stimulated emission within such a narrow spectral band can be understood analyzing the propagation of light inside the filled holes. For that, we calculated k_z in an effective manner [28], retrieving the effective refractive index of the metasurface n_{eff}, so that $k_z = n_{eff}k_0$, being k_0 the wave vector of light in vacuum. Only the zeroth diffraction order is allowed by the Bloch theorem for the lattices investigated, thus the calculated effective k_z is identical to the one obtained analytically for a metallic waveguide with circular shape [29].

Optics EXPRESS

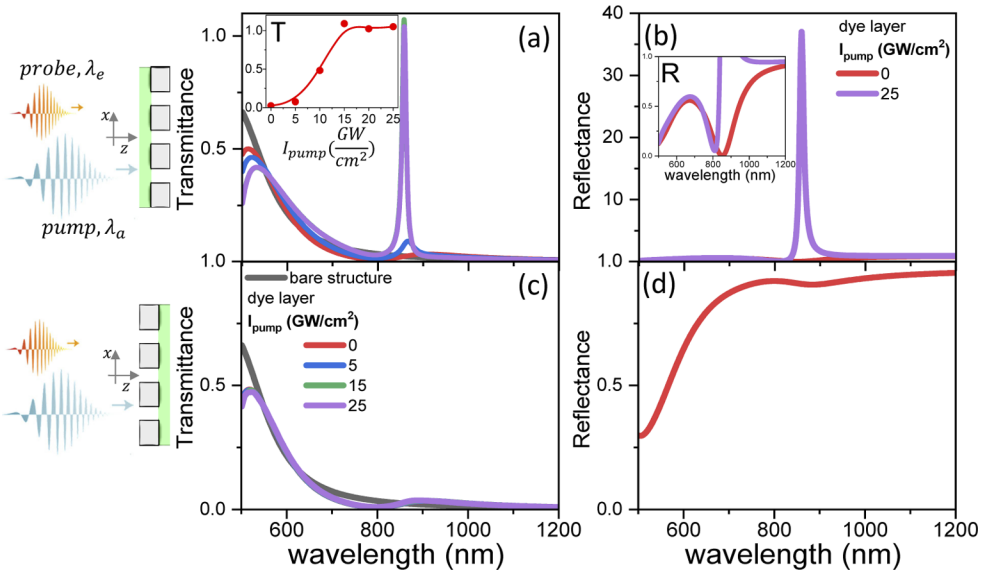

Fig. 3. Surface AIT: Probe transmittance and reflectance through an AIT metasurface (same parameters that in Fig. 2 but being $d = 220$ nm) for different pump intensities and two sample orientations. The system is pumped and probed from the same region where the IR-140 molecules are deposited in (a)-(b), while the thin slab of dye is on the other side in (c)-(d). The calculations for the bare structure (no dye at all) are shown with black lines. The inset in (a) shows the transmittance in the maximum of stimulated emission ($\lambda = 858$ nm), as a function of the pump intensity. The inset in (b) is a zoom of the main panel, highlighting the minimum of reflectance that occurs at the absorption energy of the dye for the passive case.

The first consequence of laser pumping is the reduction of the imaginary part of k_z around the emission line of the molecules λ_e, as shown in Fig. 2(d), which obviously reduces absorption at that energy.

The second effect due to the gain experienced by the metasurface, which is the most intriguing indeed, is related with the strong modification of the real part of k_z. In Fig. 2(e) an almost "vertical" slope develops as the intensity of the pump gets higher and higher values. Therefore, a slow down of the group velocity of light is produced inside the holes. The diminishing of group velocity has been arged as able to increase stimulated emission in photonic crystals [30]. We belive that a similar physical response is taken place in our case and might suggest that, like in photonic crystals, low-threshold plasmonic nanolasers might be designed based on AIT [31].

Another interesting aspect of active AIT is that in passive media (or low pump powers) AIT occurs in a three-step, non-resonant process [12]. For a resonant process to occur light must propagate back and forth inside the holes like in classical EOT [32]. In passive AIT we demonstrated that light first couples with holes, it propagates without being reflected at the second interface, exiting the metasurface as transmitted light out of the holes [12]. Reflection is the light that it is neither absorbed nor transmitted. This trend is broken for high intense illumination in gain materials. The stimulated emission peak seen in Fig. 2(c) close to λ_e can only be explained if a feedback mechanism makes the photons stay in the system enough duty cycles. It is worth to mention that no attempt to optimize the response of the AIT active metasurfaces investigated has been done in this work. We can envisage the possibility that a smart design of the cavities, formed by the holes, might provide the necessary optical feedback to sustain plasmonic lasing based on localized AIT. The trend observed in Fig. 2(f) looks promising. It shows $T + R$, the

Optics EXPRESS

fraction of light scattered from the probe in the passive case and scattered plus generated (as stimulated light) in the active case. Its dependence with pump intensity is clearly non-linear, which is characteristic of the lasing action.

3.2. Surface AIT

AIT can also take place when the molecules are not inside the holes but on the surface, because the excitation of SPPs [13]. In this case the AIT metasurface exhibit a non-linear behavior that strongly depends on the side of the metasurface that is pumped, which might provide these systems of additional capabilities resembling those of electronic active devices. Let us illustrate the last with an example. The main panels of Fig. 3 show the probe transmittance and reflectance for different pump intensities (see labels) and for two sample orientations regarding the pump-probe direction (the geometrical parameters are similar to the ones used for localized AIT, except the hole size that is $d = 220$ nm in this case). In the passive case (without pumping) light transmission is negligible near λ_e for both configurations. The red line in Fig. 3(a) demonstrates this fact. It is basically a consequence of the geometry of the bare structure, designed to be highly reflective. Nonetheless reflectance depends on the sample orientation: it is almost zero at the energy of the absorption energy of the dye when the probe illuminates directly the dye (Fig. 3(b)), while the structure efficiently reflects the light for the other orientation (Fig. 3(d)). When the system is pumped from the metal side the obtained spectra are identical to the one obtained without pumping, which means that all the lines corresponding to these calculations in Fig. 3(c) overlap. It happens the same in the case of reflectance. However, the active response shows up if we pump the dye side, clearly visible in the peaks of Fig. 3(a)-(b), near the emission energy of the IR-140 dye.

Therefore the operation modes of the AIT metasurface can be controlled by the pump. The inset of Fig. 3(a) shows the transmittance calculated in the maximum of stimulated emission ($\lambda = 858$ nm), as a function of the pump intensity. There, we can observe a transistor-like behavior defined by these operation modes: i) saturation, when the metasurface is not pumped the AIT device acts like a short circuit for the probe, ii) cut-off, the AIT device acts like an open circuit when $I_{pump}>15GW/cm^2$, being $T \sim 1$, and iii) active, for intermediate energies, so the transmittance is almost proportional to the pump intensity. We can envisage many possible uses of an AIT device for active control of light in addition to the above mentioned. These systems would allow fine control of the stimulated light emitted in transmission and in reflection regions.

At this point, it is interesting to investigate the dynamics of the atomic populations within the dye layer of the AIT metasurface, in order to understand the mechanism behind surface AIT. For that, Fig. 4(a) shows the steady-state occupation density of the emission energy level (N_2/N) within the dye layer, calculated on a unit-cell cross-cut ($y = 125$ nm), for the system and conditions investigated in Fig. 3(a). The intensity of the pump is the highest analyzed, $I_{pump} = 25\ GW/cm^2$. The 150 fs pump produces a quick change in atomic populations as can be seen in Fig. 4(b) (see caption for details), but after a while the populations reach the steady-state, considering the large relaxation time of the emission level ($\tau_{21} = 240$ ps). The gain induced by the pump is evident in Fig. 4(a) that show N_2/N exceeding the ground state density, i.e., population inversion is taken place.

The populations,through Eq. (6), serve to obtain the maps of Fig. 4(c)-(e), which show the real and imaginary parts of the dielectric constant at the emission peak in Fig. 3(a) ($\lambda = 858$ nm), for the steady-state. In addition panels (d) and (f) in the same figure represent ε_r and ε_i as a function of wavelength, at two different instants: the onset of the simulation (circles) and the steady-state (squares). All the curves were obtained in the location indicated with a circle in panel (a).

It is clear from the maps of Fig. 4 that the dielectric constant seen by the probe when reached the system, 800 fs after the pump, is quite homogeneous. This result allow us to approximate the study of the propagation constant of the SPPs excited at the hole array (the band structure), by

Optics EXPRESS

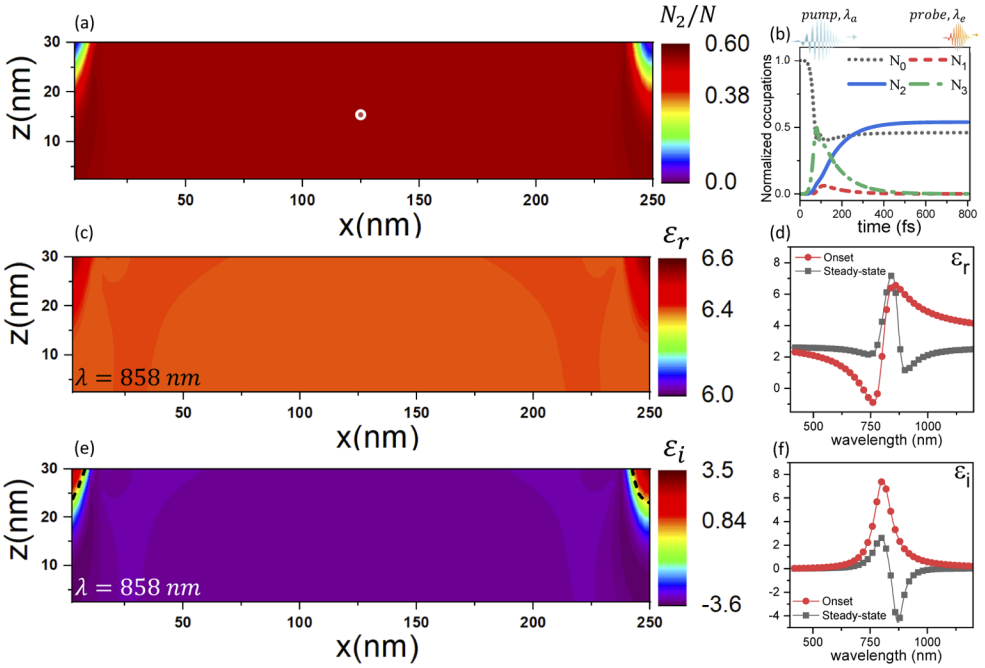

Fig. 4. For the system and conditions investigated in Fig. 3(a) and for $I_{pump} = 25\ GW/cm^2$: (a) Steady-state occupation density of the emission energy level (N_2/N) within the dye layer, calculated on a unit-cell cross-cut ($y = 125$ nm). The dye is pumped from below. (b) Time evolution of normalized populations at the location marked with a dot in (a). (c) Corresponding map of the real part of the dielectric constant (ε_r) at the emission peak seen in Fig. 3(a) , $\lambda = 858$ nm. (d) ε_r at the marked point as a function of wavelength at two different instants: the onset of the simulation (circles) and the steady-state (squares). (e)-(f) The same that in (c)-(d) but for the imaginary part. The dashed line shows in (e) $\varepsilon_i = 0$.

the modes of a simpler system, an uncorrugated silver/dye (semi-infinite medium) interface. In addition, given the extraordinary vertical confinement of the SPPs excited in the actual situation, the approximation of semi-infinite dye layer suffices to illustrate the physics behind surface AIT. The plasmonic modes are given by the following dispersion relation:

$$k_{spp}(\omega) = \frac{\omega}{c}\sqrt{\frac{\varepsilon(\omega)\varepsilon_m(\omega)}{\varepsilon(\omega) + \varepsilon_m(\omega)}} \tag{8}$$

where $\varepsilon(\omega)$ and $\varepsilon_m(\omega)$ are the dielectric constants of the gain medium and the metal, respectively.

Figure 5(a) shows the dispersion relation, $Re(k_{spp})$, of an uncorrugated silver/dye interface before (blue) and after (red) pumping the system with an intense laser. The corresponding silver/host-medium interface (before introducing the dye laser) is depicted with a gray line. In the example, a population of the upper level of the emission transition of 20% has been chosen to illustrate what it would occur in the actual structure. This value is comparable to those shown in Fig. 4(a).

The real part of the propagation constant shows a "flat" region for the active case close to the emission energy of the molecules (Fig. 5(a)), which means a reduction of the group velocity of the SPP excited regarding the passive configuration. The propagation length, $1/(2Im(k_{spp})$, as shown in Fig. 5(b), changes its value from a few nanometers in the passive case to more than $50\mu m$ in the active situation at the same energy. In the passive case damping is so high that the

Optics EXPRESS

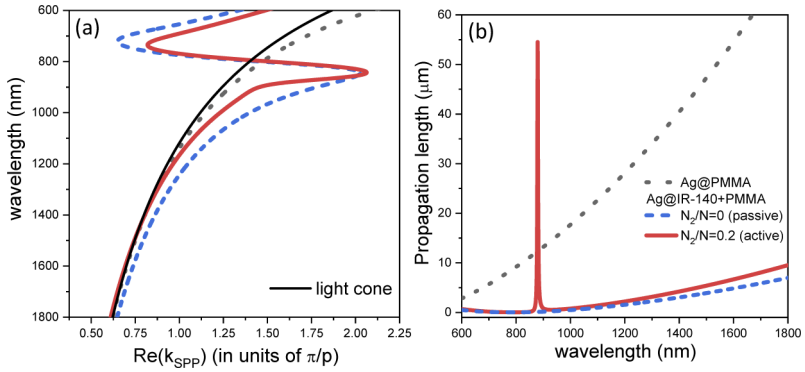

Fig. 5. (a) SPP dispersion relations calculated for: silver@PMMA (host-medium) interface (gray line); silver@IR-140+PMMA interface, before (blue) and after (red) pumping the surface with an intense laser. The emission level is populated up to 20% of the available atomic states. The black line represents the light cone. (b) Corresponding propagation constant of SPPs on the different interfaces, as a function of the wavelength.

presence of these EM modes are hidden in scattering measurements. These SPP modes suffer so strong quenching that only through Surface Plasmon Resonance experiments have been described in uncorrugated films [33]. However, the combination of a reduced group velocity and increased propagation length of SPPs, provided by the negative values of ε_i (see Fig. 4(e) - the dashed lines depict $\varepsilon_i = 0$), enhances the mechanism of active AIT and explain the results found in Fig. 3.

The paragraph above can help to explain something that has not been sufficiently considered in literature: a SPP resonance is always expected to occur at the Σ point of the band structure in arrays of nanoholes [13]. This phenomenon happens at the energy of the molecular resonance, due to the "flatness" of the dispersion relation at that energy (see Fig. 5(a)). At the end, the most feasible way to investigate these EM modes is by exploiting the gain properties of the materials, like we have done in this work.

Finally, an interesting question emerges whether or not AIT can produce lasing. To be sure that lasing action is taking place in a given device, critical information has to be obtained in terms of threshold behavior, linewidth narrowing above the threshold and spatial coherence [34]. In the present work there is some evidence regarding the potential as a plasmonic laser of the AIT platform. For instance, Fig. 2(f) shows the expected nonlinear dependence of lasing, but the kink at the threshold is not clearly seen. In addition, although spectral line narrowing is clearly observed in Fig. 2 and Fig. 3, it seems to be not enough to claim lasing, characterized by featuring much narrower peaks (<1 nm). Finally, lasing strongly depends on the geometry of the optical cavity, that defines the electromagnetic modes available for the optical feedback. In our work there is only little evidence of the effect of the cavity (holes and grating). The spectral location of the amplified stimulated light emission in the AIT metasurfaces only display a small blue-shift regarding $\lambda_e = 870$ nm, the emission wavelength of the dye. These spectral features are peaking at $\lambda = 864$ nm and $\lambda = 858$ nm in the case of localized and surface AIT, for the highest intensities of the pump beam.

4. Conclusions

We have demonstrated how AIT metasurfaces can be used to amplify stimulated emission through the modification of the optical response of an infrared dye laser deposited on top of them. An intense laser is able to modify the local dielectric constant of the gain medium, and in turn, the propagation of light either inside the holes and/or on the metal/gain-material interface. We have shown that optical transistor-like behavior could be achieved for the probe field in surface AIT

Optics EXPRESS

by externally acting on the propagation constant of SPPs. Because AIT can be found in other frequency bands, new avenues to active control in nanophotonics are possible in other spectral regimes, after this work. Finally, we believe that active AIT might be useful to build ultra-small plasmonic lasers and other active photodevices for future nanothechnology.

Funding. Ministerio de Ciencia, Innovación y Universidades (MAT2017-88358-C3-2-R (AEI/FEDER,UE)).

Disclosures. The authors declare no conflicts of interest.

Data availability. Data underlying the results presented in this paper are not publicly available at this time but may be obtained from the authors upon reasonable request.

References

1. E. Garmire, "Nonlinear optics in daily life," Opt. Express **21**(25), 30532–30544 (2013).
2. R. Brechbühler, S. J. W. Vonk, M. Aellen, N. Lassaline, R. C. Keitel, A. Cocina, A. A. Rossinelli, F. T. Rabouw, and D. J. Norris, "Compact plasmonic distributed-feedback lasers as dark sources of surface plasmon polaritons," ACS Nano **15**(6), 9935–9944 (2021).
3. R. G. Parkhomenko, A. S. Kuchyanov, M. Knez, and M. I. Stockman, "Lasing spaser in photonic crystals," ACS Omega **6**(6), 4417–4422 (2021).
4. S. Wuestner, A. Pusch, K. L. Tsakmakidis, J. M. Hamm, and O. Hess, "Overcoming losses with gain in a negative refractive index metamaterial," Phys. Rev. Lett. **105**(12), 127401 (2010).
5. R. Marani, A. D'Orazio, V. Petruzzelli, S. G. Rodrigo, L. Martín-Moreno, F. J. García-Vidal, and J. Bravo-Abad, "Gain-assisted extraordinary optical transmission through periodic arrays of subwavelength apertures," New J. Phys. **14**(1), 013020 (2012).
6. F. van Beijnum, P. J. van Veldhoven, E. J. Geluk, M. J. A. de Dood, G. W. 't Hooft, and M. P. van Exter, "Surface plasmon lasing observed in metal hole arrays," Phys. Rev. Lett. **110**(20), 206802 (2013).
7. W. Zhou, M. Dridi, J. Y. Suh, C. H. Kim, D. T. Co, M. R. Wasielewski, G. C. Schatz, and T. W. Odom, "Lasing action in strongly coupled plasmonic nanocavity arrays," Nat. Nanotechnol. **8**(7), 506–511 (2013).
8. X. Meng, J. Liu, A. V. Kildishev, and V. M. Shalaev, "Highly directional spaser array for the red wavelength region," Laser Photonics Rev. **8**(6), 896–903 (2014).
9. F. v. Beijnum, P. J. van Veldhoven, E. Jan Geluk, G. W. t. Hooft, and M. P. van Exter, "Loss compensation of extraordinary optical transmission," Appl. Phys. Lett. **104**(6), 061112 (2014).
10. O. Hess, J. B. Pendry, S. A. Maier, R. F. Oulton, J. M. Hamm, and K. L. Tsakmakidis, "Active nanoplasmonic metamaterials," Nat. Mater. **11**(7), 573–584 (2012).
11. J. A. Hutchison, D. M. O'Carroll, T. Schwartz, C. Genet, and T. W. Ebbesen, "Absorption-induced transparency," Angew. Chem. Int. Ed. **50**(9), 2085–2089 (2011).
12. S. G. Rodrigo, F. J. García-Vidal, and L. Martín-Moreno, "Theory of absorption-induced transparency," Phys. Rev. B **88**(15), 155126 (2013).
13. X. Zhong, S. G. Rodrigo, L. Zhang, P. Samorí, C. Genet, L. Martín-Moreno, J. A. Hutchison, and T. W. Ebbesen, "Waveguide and plasmonic absorption-induced transparency," ACS Nano **10**(4), 4570–4578 (2016).
14. S. G. Rodrigo, F. de León-Pérez, and L. Martín-Moreno, "Extraordinary optical transmission: Fundamentals and applications," Proc. IEEE **104**(12), 2288–2306 (2016).
15. M. F. Acosta, S. G. Rodrigo, L. Martín-Moreno, C. Pecharromán, and R. I. Merino, "Micropillar templates for dielectric filled metal arrays and flexible metamaterials," Adv. Opt. Mater. **5**(3), 1600670 (2017).
16. C. E. Petoukhoff and D. M. O'Carroll, "Absorption-induced scattering and surface plasmon out-coupling from absorber-coated plasmonic metasurfaces," Nat. Commun. **6**(1), 7899 (2015).
17. S. G. Rodrigo, "Terahertz gas sensor based on absorption-induced transparency," EPJ Appl. Metamaterials **3**, 11 (2016).
18. D. Hasan, C. P. Ho, and C. Lee, "Thermally tunable absorption-induced transparency by a quasi 3d bow-tie nanostructure for nonplasmonic and volumetric refractive index sensing at mid-ir," Adv. Opt. Mater. **4**(6), 943–952 (2016).
19. X. Li, F. Liu, M. Tian, and X. Zhong, "Tunable multimode plasmon–exciton coupling for absorption-induced transparency and strong coupling," J. Phys. Chem. C **124**(43), 23888–23894 (2020).
20. J. M. Winkler, F. T. Rabouw, A. A. Rossinelli, S. V. Jayanti, K. M. McPeak, D. K. Kim, B. le Feber, F. Prins, and D. J. Norris, "Room-temperature strong coupling of cdse nanoplatelets and plasmonic hole arrays," Nano Lett. **19**(1), 108–115 (2019).
21. D. Yoo, F. de León-Pérez, M. Pelton, I.-H. Lee, D. A. Mohr, M. B. Raschke, J. D. Caldwell, L. Martín-Moreno, and S.-H. Oh, "Ultrastrong plasmon–phonon coupling via epsilon-near-zero nanocavities," Nat. Photonics **15**(2), 125–130 (2021).
22. A. A. Rossinelli, H. Rojo, A. S. Mule, M. Aellen, A. Cocina, E. De Leo, R. Schäublin, and D. J. Norris, "Compositional grading for efficient and narrowband emission in cdse-based core/shell nanoplatelets," Chem. Mater. **31**(22), 9567–9578 (2019).

Optics EXPRESS

23. P. Sperber, W. Spangler, B. Meier, and A. Penzkofer, "Experimental and theoretical investigation of tunable picosecond pulse generation in longitudinally pumped dye laser generators and amplifiers," Opt. Quantum Electron. **20**(5), 395–431 (1988).
24. S. Wuestner, A. Pusch, K. L. Tsakmakidis, J. M. Hamm, and O. Hess, "Gain and plasmon dynamics in active negative-index metamaterials," Philos. Trans. R. Soc., A **369**(1950), 3525–3550 (2011).
25. S. G. Rodrigo, *Optical Properties of Nanostructured Metallic Systems: Studied with the Finite-Difference Time-Domain Method*, Springer Theses (Springer, 2011).
26. S. G. Rodrigo, F. J. García-Vidal, and L. Martín-Moreno, "Influence of material properties on extraordinary optical transmission through hole arrays," Phys. Rev. B **77**(7), 075401 (2008).
27. A. E. Siegman, *Lasers* (University Science Books, 1986).
28. D. R. Smith, S. Schultz, P. Markoš, and C. M. Soukoulis, "Determination of effective permittivity and permeability of metamaterials from reflection and transmission coefficients," Phys. Rev. B **65**(19), 195104 (2002).
29. J. D. Jackson, *Classical Electrodynamics 2nd edition* (Wiley, New York, 1975).
30. K. Sakoda, "Enhanced light amplification due to group-velocity anomaly peculiar to two- and three-dimensional photonic crystals," Opt. Express **4**(5), 167–176 (1999).
31. K. Sakoda, K. Ohtaka, and T. Ueta, "Low-threshold laser oscillation due to group-velocity anomaly peculiar to two- and three-dimensional photonic crystals," Opt. Express **4**(12), 481–489 (1999).
32. L. Martín-Moreno, F. J. García-Vidal, H. J. Lezec, K. M. Pellerin, T. Thio, J. B. Pendry, and T. W. Ebbesen, "Theory of extraordinary optical transmission through subwavelength hole arrays," Phys. Rev. Lett. **86**(6), 1114–1117 (2001).
33. W.-H. Yeh, J. W. Petefish, and A. C. Hillier, "Resonance quenching and guided modes arising from the coupling of surface plasmons with a molecular resonance," Anal. Chem. **84**(2), 1139–1145 (2012).
34. I. Samuel, E. Namdas, and G. Turnbull, "How to recognize lasing," Nat. Photonics **3**(10), 546–549 (2009).